Available online at www.sciencedirect.com
SCIENCE DIRECT®
PERGAMON
International Journal of Heat and Mass Transfer 47 (2004) 149–163
International Journal of HEAT and MASS TRANSFER
www.elsevier.com/locate/ijhmt

Numerical study of cavitating flow characteristics of liquid helium in a pipe

Jun Ishimoto [a,*], Kenjiro Kamijo [b]

[a] Department of Intelligent Machines and System Engineering, Hirosaki University, 3 Bunkyo-cho, Hirosaki 036-8561, Japan
[b] Institute of Fluid Science, Tohoku University, 2-1-1, Katahira, Aoba-ku, Sendai 980-8577, Japan

Received 19 August 2002

Abstract

The fundamental characteristics of the two-dimensional cavitating flow of liquid helium in a vertical pipe near the lambda point are numerically investigated to realize the further development and high performance of new cryogenic superfluid cooling systems. It is found that the phase transition of the normal fluid to the superfluid and the generation of superfluid counterflow against normal fluid flow based on the thermomechanical effect is conspicuous in the large gas phase volume fraction region where the liquid to gas phase change with cavitation actively occurs. Furthermore, it is clarified that the mechanism of the He I to He II phase transition caused by the temperature decrease is due to the deprivation of latent heat for vaporization from the liquid phase.

Keywords: Liquid helium; Cavitation; Multiphase flow; Cryogenics; Pipe flow

1. Introduction

Cryogenic flow systems or machinery that include cavitating flow or two phase flow are widely used in LNG plants, aerospace technology, superconducting magnets technology, infrared space telescope, and many other engineering applications [1,2]. Thus, the investigation of the cavitating flow or two phase flow characteristics of cryogenic fluids such as liquid helium is very interesting and important not only in the basic study of the hydrodynamics of cryogenic fluids [3], but also for providing solutions to problems related to new practical engineering applications like the new concept of multiphase superfluid cooling system using liquid helium cavitating flow. The principle of this cooling system is schematically depicted in Fig. 1. The system can realize the extensively low-temperature cooling utilizing the He I to He II phase transition based on cavitation of the normal fluid, without the direct use of He II. Additionally, the concept of multiphase superfluid cooling should be expected for development of the available micro-cooling system, such as micro-electro-mechanical systems (MEMS) technology using micro bubble [4], because the unique characteristics of zero-viscosity of superfluid working refrigerant prevents the frictional dissipation of a capillary channel in micro devices. The direct use of the He II flow encounters very difficult problems because of its production method in super low-temperature field, or super leak phenomena in transfer system, etc. Thus, it is possible to say that the application of cavitating flow of He I as a refrigerant is very useful and effective method for low-temperature cooling or cryogenic heat exchange system.

In general, cryogenic fluids are characterized by large compressibility compared with fluids at room temperature such as water, as well as by a small difference in density between the gas and liquid phases, and a small latent heat of vaporization. These unique characteristics of cryogenic fluids can be utilized to realize high performance in fluid apparatuses, such as the cavitating operation of inducers [5].

Although cryogenic fluid flow characteristics has been investigated for many years, there yielded only

* Corresponding author. Tel./fax: +81-172-393680.
E-mail address: ishimoto@cc.hirosaki-u.ac.jp (J. Ishimoto).

0017-9310/$ - see front matter © 2003 Elsevier Ltd. All rights reserved.
doi:10.1016/S0017-9310(03)00386-7

Nomenclature

c_p	specific heat at constant pressure
D	inner diameter of pipe
e	specific internal energy
$\boldsymbol{g}$	vector of gravitational acceleration
h	specific enthalpy
$\boldsymbol{I}$	unit tensor
$\boldsymbol{j}$	momentum flux density vector
k	heat transfer rate
N	number density
P	absolute pressure
R	radius of bubble or droplet
r	radial coordinate
S	specific entropy
T	absolute temperature
t	time
u	velocity component in the r-direction
v	velocity component in the z-direction
$\boldsymbol{v}$	vector of velocity
$\boldsymbol{x}$	position vector
z	longitudinal coordinate
α	void fraction
Γ	phase generation density
κ	ratio of specific heat
λ	thermal conductivity
μ	dynamic viscosity
ν	kinematic viscosity
ρ	density
σ	surface tension
θ	azimuthal coordinate
$\boldsymbol{\tau}$	viscous stress tensor
ω	vorticity
$\boldsymbol{\Omega}$	angular velocity vector
$\Re$	gas constant

Subscripts

$()_c$	condensation
$()_e$	evaporation
$()_{(ex)}$	exit section of the pipe
$()_g$	gas phase
$()^{(i)}$	interface
$()_{(in)}$	inlet section of the pipe
$()_l$	liquid phase
$()_{max}$	maximum value
$()_{(n)}$	normal fluid
$()_s$	saturation
$()_{(s)}$	superfluid
$()_r$	component in the r-direction
$()^T$	transposed matrix
$()_z$	component in the z-direction
$()_\lambda$	lambda point
$()_\theta$	component in the θ-direction

limited information on the theoretical and experimental study of the basic multiphase hydrodynamic characteristics of cavitating pipe flow of cryogenic fluids such as superfluid liquid helium [6–9]. The main reason for the difficulty in the study of cryogenic fluids is that effective formulation, modeling and numerical procedure of the governing equations for cryogenic cavitating flow with phase change have not been established. Difficulties in the experimental confirmation of cryogenic fluid under condition of a low-temperature field and the complete heat insulation of the flow pipe with measuring devices are other reasons. In particular, in the case of liquid helium, as the superfluidity in the low-temperature field less than the λ point shows extremely complex phenomena, many difficulties are encountered in the theoretical analysis. To overcome these difficulties, we herein develop a new method for analyzing cavitating flow based on an advanced mathematical model, which takes the effect of superfluidity of the cavitating cryogenic flow state in the low-temperature field into consideration.

In the present study, the two-dimensional characteristics of cavitating flow of liquid helium with phase change in a pipe are numerically investigated to realize the further development and high performance of cooling devices or new cryogenic engineering applications. First, the governing equations of the cavitating flow of liquid helium based on the unsteady multi-fluid model are presented, and then several flow characteristics are numerically calculated, taking into account the effect of superfluidity.

2. Numerical method

In the past few years, the governing equations that represent the gas–liquid two-phase mixture flow of liquid helium have been derived and numerically solved by one of the authors [10]. As a result, the two-phase flow characteristics with superfluidity have been partially clarified. In the previous analysis of two-phase flow, we used the drift-flux model, which is the analytical model for two-phase mixture flow taking into account the effect of pseudo gas–liquid relative velocity, so the effects of the momentum or energy exchange between gas and liquid phases have not strictly been considered [10]. In the present study on the cavitating flow of liquid helium, we developed a new model for analysis, which is based on the unsteady thermal nonequilibrium multi-fluid

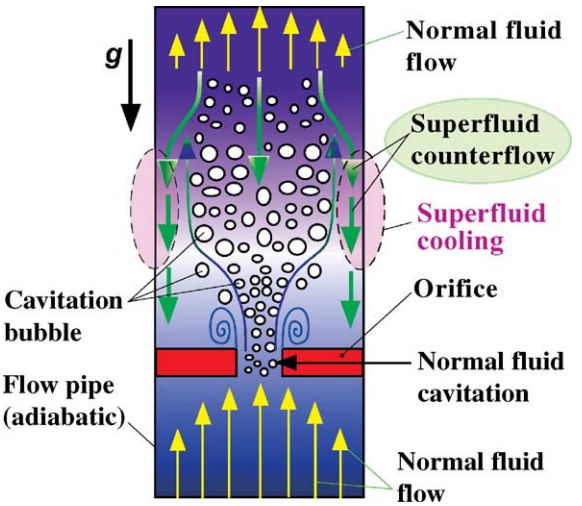

Fig. 1. Concept of multiphase superfluid cooling system using cavitating flow of liquid helium.

model by Kataoka [11]. Furthermore, to consider the effects of the evaporation and the condensation on the vapor bubbles, we apply the rapid phase change model to the cavitating flow of liquid helium with superfluidity. The system used in the numerical analysis is schematically depicted in Fig. 2. Applications using cryogenic fluid generally encounter obstacles or complex pipe shapes such as an orifice or a converging–diverging nozzle. Thus, the model used for analysis simulates the cavitating flow of liquid helium passing through the orifice of a vertical cylindrical pipe. The pipe is filled with pressurized liquid helium in adiabatic condition. Flow immediately occurs when the outlet D–C is opened. Liquid helium is continuously introduced via the inlet section A–B, the flow is accelerated at the point of the orifice, and the cavitation or liquid to vapor phase change is induced by a decrease of pressure.

2.1. Governing equations

In the present numerical formulation of the cavitating flow characteristics of liquid helium, we extend the old two-fluid model [3] to a new cryogenic vapor–liquid multiphase fluid model for analysis which is based on the unsteady thermal nonequilibrium multi-fluid model of Kataoka [11], Harlow and Amsden [12]. In the numerical model, the cryogenic cavitating flow state can be approximated to that of a homogeneous bubbly flow because the differences in the physical properties such as density, viscosity and surface tension of the cryogenic fluid between the gas and liquid phases, are very small compared with those of the fluid at room temperature. The small difference in the properties between gas and liquid phases is unique to cryogenic fluids. Accordingly, it seems reasonable to assume that the cryogenic cavitating flow pattern is easily formed in the bubbly two-phase flow.

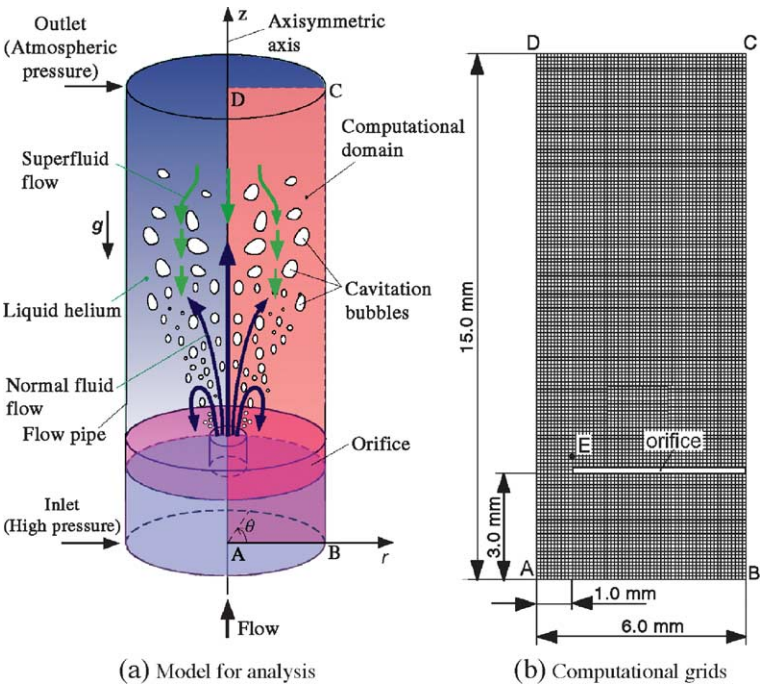

Fig. 2. Schematic of computational system used in numerical analysis.

In the process of modeling, we consider the effects of superfluidity in two-phase liquid helium, namely, superfluid He II and normal fluid He I are treated as a perfect fluid and meta-viscous fluid, respectively. In the calculation, we assume that the property of superfluidity appears when the fluid temperature becomes less than the λ point (temperature at normal fluid to superfluid transition, about $T_{l\lambda} = 2.17$ K); however, in the case of temperatures above the λ point, we assume that the superfluid behaves in the same manner as the normal fluid. Here, we consider only the temperature dependence of the superfluid and normal fluid densities; thus, the normal fluid–superfluid transition ratio based on quantum theory is not strictly considered. Furthermore, to consider the effects of the rapid evaporation and condensation of cryogenic fluid, we apply the rapid phase change model of Yamamoto et al. [13] and Young [14] to the cavitating flow of liquid helium.

The calculation is carried out using the two-dimensional cylindrical coordinate system (r, z). The model for analysis simulates the cavitating flow of liquid helium passing through the orifice of a vertical pipe. In the numerical modeling under this condition, the following assumptions are employed to formulate the governing equations.

(1) The cavitating flow is an axisymmetric two-dimensional unsteady pipe flow.
(2) The vapor gas phase is produced by the phase change of the normal fluid.
(3) The energy exchange between the liquid and gas phases is taken into account.

For the construction of the cavitating flow characteristics in the present numerical model, it is assumed that the gas phase is homogeneously dispersed in the surrounding liquid phase and that the flow structure will form a bubbly flow.

Under the above conditions, the governing equations of the cavitating flow, taking into account the effect of superfluidity based on the unsteady two-dimensional multi-fluid model, are derived as follows.

The mass conservation equation for the gas phase is

$$\frac{\partial}{\partial t}(\alpha\rho_g) + \nabla\cdot(\alpha\rho_g \boldsymbol{v}_g) = \Gamma_g. \tag{1}$$

The mass conservation equation for the liquid phase is

$$\frac{\partial}{\partial t}[(1-\alpha)\rho_l] + \nabla\cdot[(1-\alpha)\boldsymbol{j}_l] = \Gamma_l, \tag{2}$$

where the relationship $(\Gamma_g + \Gamma_l = 0)$ is assumed. The liquid phase density, ρ_l, must be comprised of a linear combination of the two components. The density is expressed by the sum of the normal fluid and superfluid components, and ρ_l is defined as follows:

$$\rho_l = \rho_{l(n)} + \rho_{l(s)}. \tag{3}$$

For the two-fluid model, it is assumed that the entire temperature dependence of liquid helium densities enter through the variation of the normal fluid density. It is therefore possible to write

$$\frac{\rho_{l(n)}}{\rho_l} = \begin{cases} \left(\dfrac{T_l}{T_{l\lambda}}\right)^{5.6} & \text{for } T_l \leqslant T_{l\lambda}, \\ 1 & \text{for } T_l > T_{l\lambda}, \end{cases} \tag{4}$$

as the temperature dependence of the normal fluid density [3]. Because of this strong temperature dependence, the He II constitutes about 99% of the superfluid component at 1.0 K. The total densities of the two components, namely, the superfluid and the normal fluid densities in control volume are conservative in the numerical calculation process. $\rho_{l(n)}$ and $\rho_{l(s)}$ are calculated by Eqs. (3) and (4) simultaneously. Also, the liquid phase momentum flux density $\boldsymbol{j}_l$ $(= \rho_l \boldsymbol{v}_l)$ can be written as the sum of each normal fluid and superfluid momentum flux density component, defined as follows:

$$\boldsymbol{j}_l = \rho_{l(s)}\boldsymbol{v}_{l(s)} + \rho_{l(n)}\boldsymbol{v}_{l(n)}. \tag{5}$$

The combined equation of motion for a total gas and normal fluid is

$$\begin{aligned} &\frac{\partial}{\partial t}[\alpha\rho_g\boldsymbol{v}_g + (1-\alpha)\rho_l\boldsymbol{v}_{l(n)}] \\ &\quad + \nabla\cdot[\alpha\rho_g\boldsymbol{v}_g\boldsymbol{v}_g + (1-\alpha)\rho_l\boldsymbol{v}_{l(n)}\boldsymbol{v}_{l(n)}] \\ &\quad = -\nabla P_l - (1-\alpha)\frac{\rho_l\rho_{l(s)}}{\rho_{l(n)}}S_l\nabla T_l - (1-\alpha)\frac{\rho_{l(s)}}{2} \\ &\qquad \times \nabla(\boldsymbol{v}_{l(n)} - \boldsymbol{v}_{l(s)})^2 + (1-\alpha)\rho_l\boldsymbol{g} \\ &\qquad + \nabla\cdot\left\{\mu_T\left[\nabla\boldsymbol{v}_{l(n)} + (\nabla\boldsymbol{v}_{l(n)})^{\mathrm{T}} - \frac{2}{3}(\nabla\cdot\boldsymbol{v}_{l(n)})\boldsymbol{I}\right]\right\} \\ &\qquad - (1-\alpha)\boldsymbol{F}_{l(sn)}. \end{aligned} \tag{6}$$

The combined equation of motion for a total gas and superfluid is

$$\begin{aligned} &\frac{\partial}{\partial t}[\alpha\rho_g\boldsymbol{v}_g + (1-\alpha)\rho_l\boldsymbol{v}_{l(s)}] + \nabla\cdot[\alpha\rho_g\boldsymbol{v}_g\boldsymbol{v}_g + (1-\alpha)\rho_l\boldsymbol{v}_{l(s)}\boldsymbol{v}_{l(s)}] \\ &\quad = -\nabla P_l + (1-\alpha)\rho_l S_l\nabla T_l + (1-\alpha)\frac{\rho_{l(n)}}{2}\nabla(\boldsymbol{v}_{l(n)} - \boldsymbol{v}_{l(s)})^2 \\ &\qquad + (1-\alpha)\rho_l\boldsymbol{g} + (1-\alpha)\boldsymbol{F}_{l(sn)}, \end{aligned} \tag{7}$$

where the second terms on the right-hand side of Eqs. (6) and (7) denote the thermomechanical effect of the force based on the product of the entropy by the temperature gradient, and the third terms denote the effect of the momentum energy gradient based on the two-phase superfluid–normal fluid relative velocity caused by counterflow of the superfluid against the normal fluid. The terms mentioned above are peculiar to liquid helium

with superfluidity [3]. The signs of these terms in Eq. (6) are opposite with those in Eq. (7); thus, the forces based on the superfluidity of Eq. (6) act in the direction opposite those of Eq. (7). In this calculation, because the vapor phase is assumed to be produced by the phase change of the normal fluid, the cavitating flow of the superfluid is consists of the mixture flow of the vapor phase produced by the normal fluid and the superfluid. The term $\boldsymbol{F}_{\mathrm{l(sn)}}$ denotes the two-phase superfluid–normal fluid mutual friction interaction term based on the generation of vortex filaments in the superfluid [15–17]. Assuming that the flow field is axisymmetric two-dimensional results in the following simplified formula for each r- and z-direction components of $\boldsymbol{F}_{\mathrm{l(sn)}}$:

$$F_{\mathrm{l(sn)}r} = -B\frac{\rho_{\mathrm{l(n)}}}{2}(-\omega_{\mathrm{l}\theta}v_{\mathrm{l(n)}} + \omega_{\mathrm{l}\theta}v_{\mathrm{l(s)}}), \tag{8}$$

$$F_{\mathrm{l(sn)}z} = -B\frac{\rho_{\mathrm{l(n)}}}{2}(\omega_{\mathrm{l}\theta}u_{\mathrm{l(n)}} - \omega_{\mathrm{l}\theta}u_{\mathrm{l(s)}}), \tag{9}$$

$$\omega_{\mathrm{l}\theta} = \left(\frac{\partial u_{\mathrm{l}}}{\partial z} - \frac{\partial v_{\mathrm{l}}}{\partial r}\right), \tag{10}$$

where coefficient B denotes the mutual friction parameter which has a strong temperature dependence [17].

Additionally, μ_T in Eq. (6) denotes the viscosity of the two-phase mixture flow that includes small dispersed bubbles. μ_T was evaluated using the following formula by Einstein for the viscosity of a suspension [18,19]:

$$\mu_T = (1 + 2.5\alpha)\mu_{\mathrm{l(n)}}, \tag{11}$$

where Eq. (11) being mainly applicable in the small gas phase volume fraction region. Concerning the viscosity, the present numerical model assumes that superfluid viscosity $\mu_{\mathrm{l(s)}} = 0$ and that the dissipative interaction is due only to the normal fluid. This assumption corresponds to the physical fact that the superfluid experiences no resistance to flow and therefore no turbulence. The superfluid can flow through a pipe without viscous drag along the boundaries. Equations (6) and (7) above are derived by complying the equations of momentum for both the gas and liquid phases.

To consider the effects of additional forces that act on the bubbles and radial expansion of the bubbles, the equation of motion for the gas phase is here replaced with the translational motion of a single bubble [20]. Therefore, the Eulerian–Lagrangian two-way coupling model [21] is applied to predict the two-dimensional cavitating flow characteristics. If the bubbles exist in the superfluid region, the viscous drag force $\boldsymbol{F}_{\mathrm{D}}$ that act on the bubbles in the superfluid are neglected because of the zero viscosity.

The equation of motion for the gas phase is

$$\frac{4}{3}\pi\rho_{\mathrm{g}}R_{\mathrm{g}}^3\frac{\mathrm{d}\boldsymbol{v}_{\mathrm{g}}}{\mathrm{d}t} = -\boldsymbol{F}_{\mathrm{P}} + \boldsymbol{F}_{\mathrm{g}} - \boldsymbol{F}_{\mathrm{D}} - \boldsymbol{F}_{\mathrm{VM}} - \boldsymbol{F}_{\mathrm{B}} + \boldsymbol{F}_{\mathrm{LM}} + \boldsymbol{F}_{\mathrm{LS}}, \tag{12}$$

where each additional force term is derived as follows:

$$\boldsymbol{F}_{\mathrm{P}} = \frac{4}{3}\pi R_{\mathrm{g}}^3\nabla P_{\mathrm{l}}, \tag{13}$$

$$\boldsymbol{F}_{\mathrm{g}} = \frac{4}{3}\pi R_{\mathrm{g}}^3\rho_{\mathrm{g}}\boldsymbol{g}, \tag{14}$$

$$\boldsymbol{F}_{\mathrm{D}} = \frac{1}{2}\rho_{\mathrm{l}}C_{\mathrm{D}}|\boldsymbol{v}_{\mathrm{g}} - \boldsymbol{v}_{\mathrm{l}}|(\boldsymbol{v}_{\mathrm{g}} - \boldsymbol{v}_{\mathrm{l}})\pi R_{\mathrm{g}}^2, \tag{15}$$

$$\boldsymbol{F}_{\mathrm{VM}} = C_{\mathrm{VM}}\cdot\rho_{\mathrm{l}}\frac{4}{3}\pi R_{\mathrm{g}}^3\left[\frac{\mathrm{d}}{\mathrm{d}t}(\boldsymbol{v}_{\mathrm{g}} - \boldsymbol{v}_{\mathrm{l}}) + \frac{3}{R_{\mathrm{g}}}(\boldsymbol{v}_{\mathrm{g}} - \boldsymbol{v}_{\mathrm{l}})\frac{\mathrm{d}R_{\mathrm{g}}}{\mathrm{d}t}\right], \tag{16}$$

$$\boldsymbol{F}_{\mathrm{B}} = 6R_{\mathrm{g}}^2\sqrt{\pi\rho_{\mathrm{l}}\mu_{\mathrm{l(n)}}}\int_0^t\frac{\frac{\mathrm{d}}{\mathrm{d}\tau}(\boldsymbol{v}_{\mathrm{g}} - \boldsymbol{v}_{\mathrm{l}})}{\sqrt{t-\tau}}\,\mathrm{d}\tau, \tag{17}$$

$$\boldsymbol{F}_{\mathrm{LM}} = \pi R_{\mathrm{g}}^3\rho_{\mathrm{l}}(\boldsymbol{\Omega}_{\mathrm{g}} - \boldsymbol{\Omega}_{\mathrm{l}})\times(\boldsymbol{v}_{\mathrm{g}} - \boldsymbol{v}_{\mathrm{l}}), \tag{18}$$

$$\boldsymbol{F}_{\mathrm{LS}} = 6.46\frac{\mu_{\mathrm{l(n)}}R_{\mathrm{g}}^2}{\sqrt{|(\boldsymbol{\Omega}_{\mathrm{g}} - \boldsymbol{\Omega}_{\mathrm{l}})|\nu_{\mathrm{l(n)}}}}(\boldsymbol{\Omega}_{\mathrm{g}} - \boldsymbol{\Omega}_{\mathrm{l}})\times(\boldsymbol{v}_{\mathrm{g}} - \boldsymbol{v}_{\mathrm{l}}), \tag{19}$$

$$\boldsymbol{\Omega}_{\mathrm{l}} = \frac{1}{2}\nabla\times\boldsymbol{v}_{\mathrm{l}}, \tag{20}$$

where $\boldsymbol{v}_{\mathrm{l}} = \boldsymbol{j}_{\mathrm{l}}/\rho_{\mathrm{l}}$, R_{g} is the equivalent bubble diameter, $\boldsymbol{F}_{\mathrm{P}}$ is the force due to the liquid phase pressure gradient, $\boldsymbol{F}_{\mathrm{g}}$ is the gravitational acceleration force, $\boldsymbol{F}_{\mathrm{D}}$ is the viscous drag force. $\boldsymbol{F}_{\mathrm{D}}$ is only considered while the bubble exists in the normal fluid region, and is not considered while the bubble exists in the superfluid region. $\boldsymbol{F}_{\mathrm{VM}}$ is the virtual mass force considering the expansion of a bubble, and $\boldsymbol{F}_{\mathrm{B}}$ is the Basset history term which takes into account the effect of the deviation in flow pattern from the steady state. $\boldsymbol{F}_{\mathrm{LM}}$ is the Magnus lift force caused by the rotation of the bubble as reported by Auton et al. [22]. $\boldsymbol{F}_{\mathrm{LS}}$ is Saffman's lift force [23] caused by the velocity gradient of the liquid phase. C_{D} is the drag coefficient and C_{VM} is the virtual mass coefficient. $\mathrm{d}/\mathrm{d}t$ denotes the substantial derivative.

The equation for the angular velocity of a bubble is derived as follows [23]:

$$\frac{\mathrm{d}\boldsymbol{\Omega}_{\mathrm{g}}}{\mathrm{d}t} = \frac{15\mu_{\mathrm{l(n)}}}{R_{\mathrm{g}}^2\cdot\rho_{\mathrm{g}}}(\boldsymbol{\Omega}_{\mathrm{l}} - \boldsymbol{\Omega}_{\mathrm{g}}), \tag{21}$$

The energy equation for the gas phase is

$$\begin{aligned}&\frac{\partial}{\partial t}(\alpha\rho_{\mathrm{g}}e_{\mathrm{g}}) + \nabla\cdot(\alpha\rho_{\mathrm{g}}e_{\mathrm{g}}\boldsymbol{v}_{\mathrm{g}})\\ &\quad= -P_{\mathrm{g}}\frac{\partial\alpha}{\partial t} - \nabla\cdot(\alpha P_{\mathrm{g}}\boldsymbol{v}_{\mathrm{g}}) + \Gamma_{\mathrm{g}}h_{\mathrm{g}}^{(\mathrm{i})} + q_{\mathrm{g}}^{(\mathrm{i})}a^{(\mathrm{i})} - \nabla\cdot(\alpha\boldsymbol{q}_{\mathrm{g}}) + \alpha\Phi_{\mathrm{g}}.\end{aligned} \tag{22}$$

The energy equation for the liquid phase is

$$\begin{aligned}&\frac{\partial}{\partial t}[(1-\alpha)\rho_{\mathrm{l}}e_{\mathrm{l}}] + \nabla\cdot[(1-\alpha)\rho_{\mathrm{l}}e_{\mathrm{l}}\boldsymbol{v}_{\mathrm{l}}]\\ &\quad= -P_{\mathrm{l}}\frac{\partial(1-\alpha)}{\partial t} - \nabla\cdot[(1-\alpha)P_{\mathrm{l}}\boldsymbol{v}_{\mathrm{l}}] + \Gamma_{\mathrm{l}}h_{\mathrm{l}}^{(\mathrm{i})}\\ &\qquad+ q_{\mathrm{l}}^{(\mathrm{i})}a^{(\mathrm{i})} - \nabla\cdot[(1-\alpha)\boldsymbol{q}_{\mathrm{l}}] + (1-\alpha)\Phi_{\mathrm{l}},\end{aligned} \tag{23}$$

where $h_g^{(i)}$ and $h_l^{(i)}$ are the enthalpy of the gas phase and the liquid phase at the interface, respectively. $a^{(i)}$ is the interfacial area concentration. $\Gamma_g h_g^{(i)}$ and $\Gamma_l h_l^{(i)}$ are the interfacial energy transfer terms due to the liquid–vapor phase change. $q_g^{(i)}$ and $q_l^{(i)}$ are the heat transfer terms of mutual interaction between the vapor and liquid interface. $\boldsymbol{q}$ is the heat flow vector and Φ is the energy dissipation function, as described below:

$$\begin{cases} \boldsymbol{q}_m = -\lambda_m \nabla T_m, \\ \Phi_m = \boldsymbol{\tau}_m : \nabla \boldsymbol{v}_m, \\ \boldsymbol{\tau}_m = \mu_m \left[\nabla \boldsymbol{v}_m + (\nabla \boldsymbol{v}_m)^T - \frac{2}{3}(\nabla \cdot \boldsymbol{v}_m)\boldsymbol{I} \right], \end{cases} \tag{24}$$

where subscript m denotes the gas phase (m = g) or liquid phase (m = l). In the condition of the He II state, Gorter–Mellink 1/3 power law [3,8] is considered to formulate the expression for λ_l in Eq. (24) by the following equation:

$$\lambda_l = \left(\frac{f^{-1}(T_l)}{|\nabla T_l|^2} \right)^{1/3}, \tag{25}$$

where $f(T_l)$ is the He II heat conductivity function which exhibits strong temperature dependence [3].

Assuming that the mass of each vapor bubble and of the condensed liquid droplet in each computational location is constant results in the following mass conservation equation for number density, N_k:

$$\frac{\partial}{\partial t}\left(\frac{4}{3}\pi R_k^3 N_k \rho_k \right) + \nabla \cdot \left(\frac{4}{3}\pi R_k^3 N_k \rho_k \boldsymbol{v}_k \right) = \Gamma_k, \tag{26}$$

$$\begin{cases} k = e: \ R_k = R_g, \ N_k = N_g, \ \rho_k = \rho_g, \ \boldsymbol{v}_k = \boldsymbol{v}_g, \ \Gamma_k = \Gamma_g, \\ k = c: \ R_k = R_l, \ N_k = N_l, \ \rho_k = \rho_l, \ \boldsymbol{v}_k = \boldsymbol{v}_l, \ \Gamma_k = \Gamma_l, \end{cases}$$

where subscript k denotes evaporation (k = e) or condensation (k = c).

The governing equations of cavitating flow mentioned above are constructed by Eulerian-type equations for the liquid phase and by Lagrangian-type equations for the gas phase.

2.2. Constitutive equations

It was found that the quantum cavitation with quantum tunneling remarkably occurs in the ultimate low-temperature condition of $T_l \leqslant 0.6$ K. Above $T_l = 0.6$ K, it may be possible to say that the formulation of the two phase constitutive equations for cryogenic fluid can be expected for the ordinary two phase constitutive equations for room temperature fluid [24,25].

The drag coefficient, C_D, and the virtual mass coefficient, C_{VM} in (12), are defined as follows [23]:

$$C_D = \frac{24}{Re_B}(1 + 0.15 Re_B^{0.687}) + \frac{0.42}{1 + 42500\, Re_B^{-1.16}}, \tag{27}$$

$$C_{VM} = 0.5, \tag{28}$$

$$Re_B = \frac{\rho_l |\boldsymbol{v}_g - \boldsymbol{v}_l| D}{\mu_{l(n)}}, \tag{29}$$

where C_D and Re_B are applicable while the bubbles exist in the normal fluid region. D is the inner diameter of the pipe, Re_B is the two phase Reynolds number. The energy balance condition through the interface of the gas and liquid phases is expressed by the following equation:

$$\Gamma_g h_g^{(i)} + q_g^{(i)} + \Gamma_l h_l^{(i)} + q_l^{(i)} = 0, \tag{30}$$

where $h_k = c_{pk} T_k$; (k = g, l). The constitutive equations for interfacial transfer term $q_g^{(i)}$ in Eqs. (22) and (30) are given by following cryogenic extended empirical formulas [26,27]:

$$q_g^{(i)} = k^{(i)}(T_g - T_s), \tag{31}$$

where $k^{(i)}$ is the interfacial heat transfer rate between gas and liquid phases, and is given by following equations [26]:

$$\begin{cases} k^{(i)} = \alpha k_g^{(i)} + (1-\alpha) k_{l(n)}^{(i)} \quad \text{(in normal fluid region)}, \\ k^{(i)} = \alpha k_g^{(i)} + (1-\alpha) k_{l(s)}^{(i)} \quad \text{(in superfluid region)}, \\ k_g^{(i)} = \dfrac{8.067 \cdot \lambda_g}{R_g}, \\ k_{l(n)}^{(i)} = \dfrac{1.0 + 0.37\, Re_V^{0.50} Pr_V^{0.35}}{R_g}, \\ k_{l(s)}^{(i)} = \dfrac{1}{R_g}, \\ Re_V = \dfrac{2.0 R_g |\boldsymbol{v}_g - \boldsymbol{v}_l|}{\nu_{l(n)}}, \\ Pr_V = \dfrac{c_{pl} \cdot \mu_{l(n)}}{\lambda_l}. \end{cases} \tag{32}$$

In the formulation of the above constitutive equations concerning with the interfacial transfer term, it is assumed that the energy transfer is caused by the heat transfer between the isothermal spherical bubble and the surrounding liquid. Assuming a spherical bubble with equivalent radius R_g, the expression of interfacial area concentration is obtained by the following equation [11]:

$$a^{(i)} = \frac{3\alpha}{R_g}. \tag{33}$$

Assuming that the vapor gas phase follows an ideal gas law and that the relationship between gas phase pressure, P_g, and density, ρ_g, obeys polytropic change, the following equation by Hirt and Romero [28] results:

$$\rho_g(\kappa_g - 1)e_g = [P_g - c_0^2 \rho_l(\alpha^* - \alpha)]\alpha^*, \tag{34}$$

$$\begin{cases} \alpha \geqslant \alpha_c \ : \ \alpha^* = \alpha, \\ \alpha < \alpha_c \ : \ \alpha^* = \alpha_c, \end{cases}$$

where c_0 is the first sound velocity in liquid helium at the initial state ($c_0 = 236.1$ m/s) and α_c denotes the threshold of the void fraction ($\alpha_c = 0.005$). The tables of the thermophysical properties of liquid helium by Maynard [29], Brooks and Donnelly, [30] and McCarty [31] give the required physical properties of the liquid phase.

The constitutive equation for gas phase generation density, Γ_g, is defined by the following equation:

$$\Gamma_g = \Gamma_{ge} - \Gamma_{gc}, \tag{35}$$

where Γ_{ge} and Γ_{gc} denote the gas phase evaporation density and gas phase condensation density, respectively. By introducing constitutive equations for Γ_{ge} and Γ_{gc}, we extend the classical nucleation theory for water droplets from subcooled vapor to the liquid helium. Namely, Γ_{ge} and Γ_{gc} are assumed to be proportional to the degree of subcooling and superheat. The classical nucleation theory without quantum effect can be applied to the present numerical model because the temperature range which has been dealt with this calculation is about $T_l = 2.1$ to 2.3 K (near the λ point) [24,25].

Furthermore, if Γ_{gk} (k = e, c) is expressed by the sum of the nucleation rate of the evaporated bubble or the condensed liquid droplet, and also expressed by the increase in mass due to the growth of vapor bubbles and condensed droplets, the following equations for Γ_{gk} are derived [13,14]:

$$\Gamma_{gk} = \frac{4}{3}\pi\rho_k I_k R_{k(cr)}^3 + 4\pi\rho_k \sum_{i=1}^{i_{max}} N_{ki} R_{ki}^2 \frac{dR_{ki}}{dt}, \tag{36}$$

$$\begin{cases} I_k = \dfrac{A_c}{1+\Theta}\left(\dfrac{2\sigma_l}{\pi m^3}\right)^{1/2}\dfrac{\rho_g^2}{\rho_l}\exp\left(-\dfrac{4\pi R_{k(cr)}^2\sigma_l}{3k_B T_k}\right), \\ \Theta = \dfrac{2(\kappa_g-1)}{\kappa_g+1}\dfrac{\Delta h}{\Re T_g}\left(\dfrac{\Delta h}{\Re T_g}-0.5\right), \\ R_{k(cr)} \approx \dfrac{2\sigma_l T_s}{\rho_k \Delta h \Delta T}. \end{cases}$$

In Eq. (36), subscript k has the same definition as that used in Eq. (26), R_k is the radius of a bubble or droplet, $R_{k(cr)}$ is the Kelvin–Helmholtz critical nucleate radius, k_B is Boltzmann's constant, I_k is the nuclei generation rate of vapor bubbles or liquid droplets, A_c is the condensation coefficient, Θ is the nonisothermal correction factor, m is the mass of a single molecule of helium, T_s is the saturation temperature, σ is the surface tension, $\Re$ is the gas constant, and subscript i is the value at each calculation cell. Δh denotes the latent heat which is described by the difference in specific enthalpy between the liquid and gas phases and is defined as $\Delta h = h_l - h_g$. The temperature difference between saturation temperature and gas phase temperature, ΔT, is defined as $\Delta T = T_s - T_g$. N_{ki} denotes the number density of the generated vapor bubbles or condensed liquid droplets at each calculation cell i.

By introducing the formulation of the growth process for bubbles and condensed droplets, we assume that the growth rate of a bubble or droplet is controlled by the rate at which the enthalpy of vaporization or condensation can be conducted away from the bubble and droplets to the bulk liquid [32]. Under that assumption, the equation of the growth process for a single vapor bubble and a condensed droplet is derived as

$$\Delta h \rho_k \frac{dR_{ki}}{dt} = \frac{P_k}{\sqrt{2\pi\Re T_k}}\frac{\kappa_k+1}{2\kappa_k} c_{pk}\Delta T^{(i)}, \tag{37}$$

where $\Delta T^{(i)}$ denotes the interfacial temperature between the vapor phase and the condensed droplet and is derived by the following equation:

$$\Delta T^{(i)} = \left(1 - \frac{R_{k(cr)}}{R_{ki}}\right)(T_s - T_g). \tag{38}$$

2.3. Numerical conditions and procedure

To construct the numerical conditions for the cavitating liquid helium flow, we refer to the cryogenic cavitating internal flow state or condition of the liquid helium cavitating flow in a venturi channel reported by Ishii and Murakami [6], Daney [7], and to the LE-7 liquid oxygen turbopump for the H-II rocket engine reported by Kamijo et al. [5]. The finite difference method is used to solve the set of governing equations mentioned above. In the present calculation, the discrete forms of these equations are obtained using a staggered grid; then the modified SOLA (numerical SOLution Algorithm for transient fluid flow) method of Tomiyama and Hirano [33], which is superior for the formulation and solution of a gas liquid two-phase flow problem, is applied for the numerical calculation. The liquid phase velocity, $\boldsymbol{v}_l$, at the location of bubbles is calculated using an area-weighting interpolation method which was used in the SMAC algorithm by Amsden and Harlow [34].

To determine the boundary conditions, free-slip conditions for prescribed superfluid and normal fluid velocities are applied to the axisymmetric axis, D–A, in Fig. 2. Nonslip conditions for prescribed normal fluid velocities and free-slip conditions for prescribed superfluid velocities are applied to the sidewall, C–B. Also, a fully developed velocity profile is applied for normal fluid velocities to the inlet cross-sectional area of the flow pipe, A–B. A convective outflow condition is applied to the exit section of the pipe, D–C. Adiabatic conditions are applied for thermal boundary conditions at the pipe wall surface. The initial stationary condition of the liquid phase is assumed to be the pressurized He I state. Also, the initial conditions at the inlet section of the flow pipe are as given in Table 1. For other physical properties used in constitutive equations, $\mu_{l(n)}$ and S_l are given as functions of temperature [29–31].

Table 1
Conditions for numerical analysis

Inlet pressure	$P_{l(in)}$	0.20	MPa
Outlet pressure	$P_{l(ex)}$	0.101	MPa
Internal energy	$e_{l(in)}$	6.021	kJ/kg
Inner diameter of pipe	D	10.0	mm

The interval of each time step is automatically adjusted during the computation to satisfy the CFL condition. We actually calculated solutions on three different grid densities: 50×120, 60×150 and 110×220 nodes. As a result, we found that numerical results for all three grids show the same profiles, and the grid independence of the numerical results was confirmed. Thus, as a compromise between computer memory and accuracy, we chose to use the 60×150 grid (6.0 mm $\times$ 15.0 mm, physical dimensional computational domain) in the r- and z-directions for the calculations. The calculation is executed until an almost steady state of the cavitating flow is attained.

2.4. Results and discussion

Fig. 3 shows the numerical results of the transient evolution of the void fraction (α) contour, Fig. 4 shows the transient evolution of the liquid phase temperature (T_l) contour, and Fig. 5 shows the instantaneous liquid phase pressure (P_l) contour. The direction of mainstream is upward longitudinal direction. Fig. 6 shows the fluctuations of void fraction, α and pressure, P_l as a function of the time at position E ($r = 1.0$ mm, $z = 3.3$ mm, as depicted in Fig. 2) just downstream of the orifice, where the cavitation actively occurs. Fig. 7 shows the fluctua-

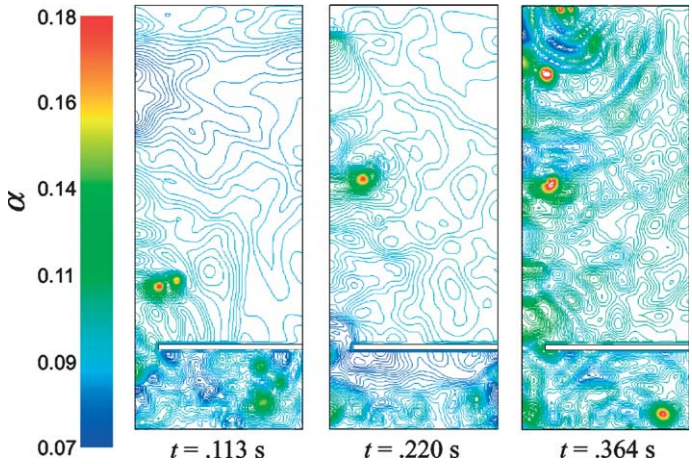

Fig. 3. Time evolution of void fraction distributions.

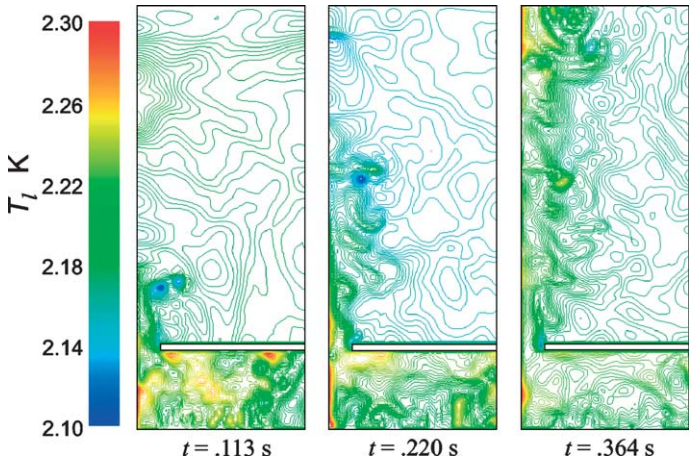

Fig. 4. Time evolution of liquid phase temperature profiles.

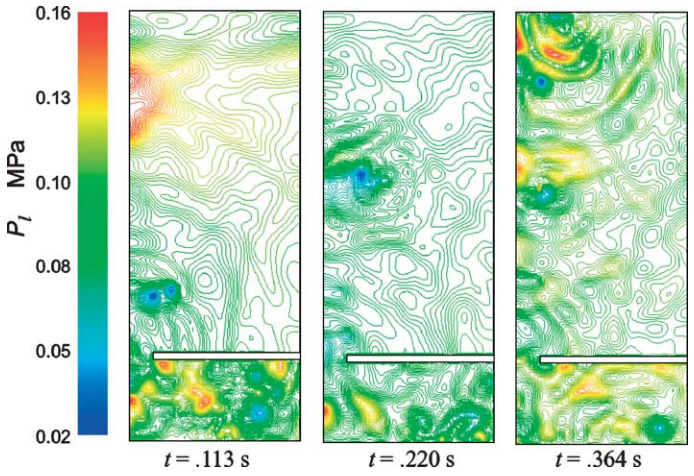

Fig. 5. Instantaneous liquid phase pressure contours.

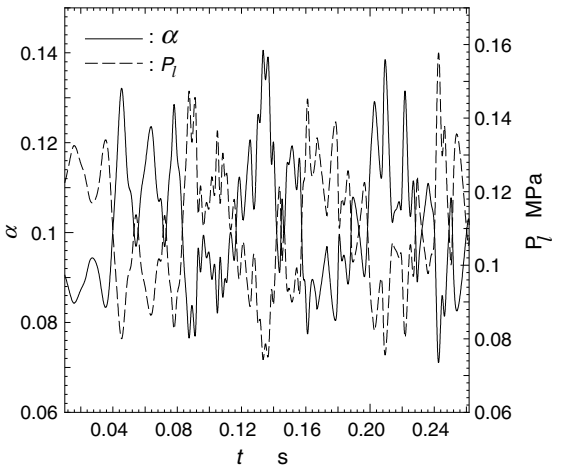

Fig. 6. Fluctuations of void fraction and liquid phase pressure as a function of time.

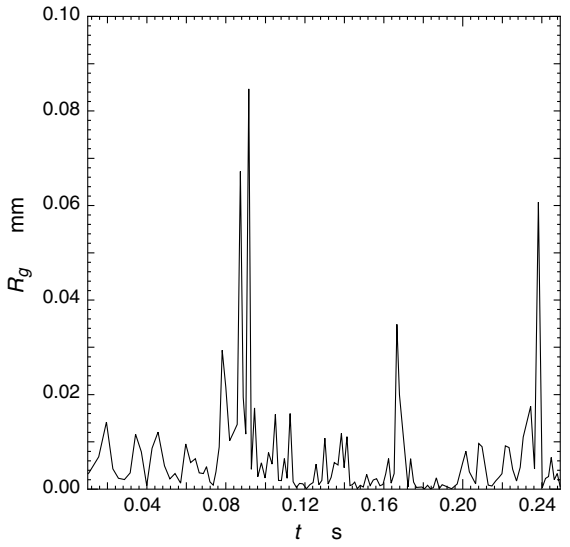

Fig. 7. Fluctuations of bubble radius as a function of time.

tion of bubble radius, R_g as a function of the time at position E. As shown by Fig. 3, it is clear that the phase change with cavitation effectively occurs with time and the cavity vortices are formed, and that the gas phase advects and spreads throughout the inner flow pipe. In this numerical calculation, it is assumed that the existence of the large gas phase volume fraction region indicates that the small size bubbles shown in Fig. 7 constitute a closely aggregated region and that the downstream flow state keeps very closed bubbly flow in the large void fraction region. The bubbles are concentrated toward the center of the vortex cavity due to the negative pressure gradient in the vortex.

It is found that the characteristics of superfluidity are conspicuous in the large gas phase volume fraction region where the phase change with cavitation actively occurs and the pressure gradient actively changes. The effect of superfluidity with He I to He II phase transition is mainly caused by the decrease in liquid phase temperature or internal energy due to the deprivation of latent heat for vaporization from the liquid phase and to the change of the specific heat of the liquid phase with the change of pressure gradient. From Fig. 4, it is especially found that the temperature around the interface between the large gas phase volume fraction region and the liquid phase region decreases with the increase in the phase change. The liquid phase temperature decrease due to the latent heat, or the energy exchange between liquid- and vapor phase in the vaporization process are characterized by the interfacial energy transfer terms with the phase change in Eqs. (22) and (23).

From Figs. 3–7, it is clarified that the decrease of P_l induces the increase of α, and the expansion or contraction of bubble radius R_g correspond to the change of P_l, however, the displacement magnitude of R_g shows small value. Thus, it is also clarified that the generated cavitation bubbles keep small size in the vaporization process and in the initial cavitating flow state. Furthermore, in the region of high volume fraction of the gas phase, the pressure distribution changes markedly because of the normal fluid–superfluid transition due to the momentum terms in Eqs. (6) and (7) that include the temperature gradient term, the momentum energy gradient term based on relative superfluid–normal fluid velocity, and the superfluid–normal fluid mutual friction interaction term.

Focusing on Figs. 3 and 6, the decrease in the absolute value of the negative pressure gradient and the increase in the absolute value of the positive pressure gradient with time are found near the downstream region passing through the orifice. Immediately after the flow is initially induced, taking note of the primary feature of the void fraction profile, the gas phase leaves from a position behind the edge of the orifice and is concentrated downstream of orifice due to the small vortex induced by the He I wake passing through the orifice, based on the effect of the negative pressure gradient. With time, the gas phase rises from the edge of the orifice, and the high volume fraction region of the gas phase advects downstream. It is found that the phase change with cavitation effectively occurs with time and that the gas phase spreads throughout the inner flow pipe, because of the decrease in the slip ratio and the gas phase velocity resulting from the sudden change of both longitudinal and transverse pressure gradients based on the superfluidity generation. Another reason for the enhancement of liquid–vapor phase change is that the existence rate of the gas phase spread in the pipe per unit time increases with the increase in the effect of superfluidity. The tendencies of those numerical results for void fraction profiles, pressure distribution, and temperature decrease with the He I to He II phase transition show qualitative agreement with the experimental datum on the He I cavitation in the saturated condition by Ishii and Murakami [6].

Figs. 8–10 show profiles of the instantaneous liquid phase normal fluid velocity component $\boldsymbol{v}_{l(n)}$, the superfluid velocity component $\boldsymbol{v}_{l(s)}$, and gas phase velocity $\boldsymbol{v}_g$, respectively. Fig. 11 shows the velocity fluctuations of normal fluid and superfluid as a function of the time at the position E. In the case of temperatures above the λ point, we assume that the superfluid behaves in the same manner as the normal fluid; thus the profile of $\boldsymbol{v}_{l(s)}$ similar to the profile of $\boldsymbol{v}_{l(n)}$ denotes the normal fluid velocity profile. Concerning with Figs. 5 and 8, it is found that there is a low-pressure region passing through the central axis of the orifice induced by the acceleration of fluid velocity. From Fig. 8, it can be seen that the magnitude of fluctuation of $\boldsymbol{v}_{l(n)}$ increases with an increase in longitudinal coordinate z just behind the orifice.

From a comparison of the results of the two-phase velocity profile between the $\boldsymbol{v}_{l(n)}$ and $\boldsymbol{v}_{l(s)}$, it is clear that the counterflow or counter-vortex of the superfluid against the normal fluid occurs in the region where the liquid to vapor phase change with cavitation actively occurs; and that the velocity vectors between normal fluid and superfluid show different profiles. Immediately after the flow is initially induced, taking note of the primary feature of the liquid phase velocity profile, profiles of $\boldsymbol{v}_{l(n)}$ and $\boldsymbol{v}_{l(s)}$ behave similarly; however, the rotating direction of the each vortices is opposite. With time, especially downstream of the orifice in the high

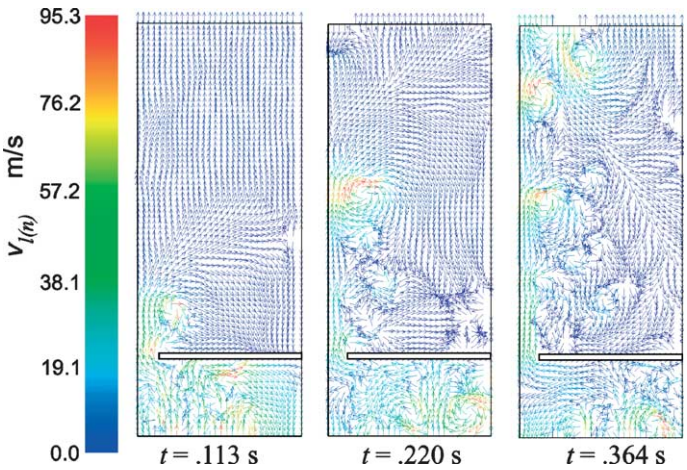

Fig. 8. Instantaneous normal fluid velocity vector.

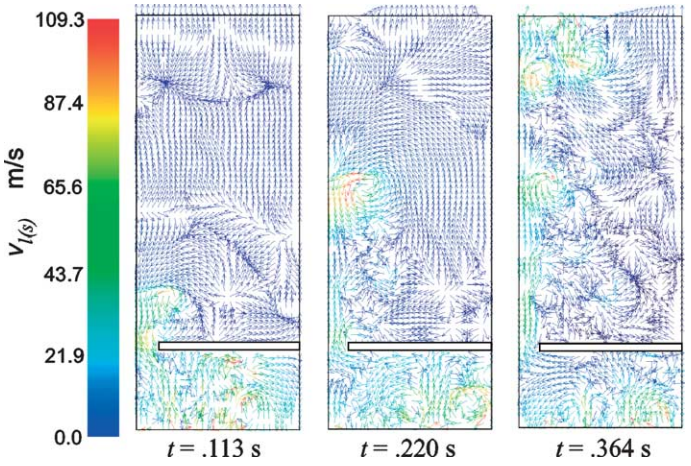

Fig. 9. Instantaneous superfluid velocity vector.

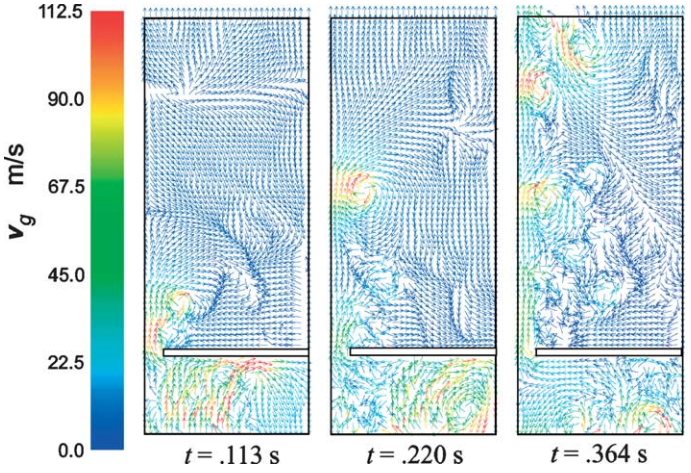

Fig. 10. Instantaneous gas phase velocity vector.

volume fraction region of the gas phase, the difference in velocity profiles is observed due to the counterflow of the superfluid against the normal fluid based on the generation of the superfluidity.

Also, it is found that the magnitude of the vortex induced by the normal fluid wake passing through the orifice becomes larger; however, the vortex has a shape different from that of superfluid because of the slight viscosity in normal fluid and counterflow of superfluid. The superfluid counterflow against normal fluid is mainly caused by the momentum terms in Eqs. (6) and (7), i.e., the temperature gradient term (thermomechanical effect) and the momentum energy gradient term for superfluid–normal fluid relative velocity. The mechanism for thermomechanical effect of the superfluid counterflow or counter-vortex generation due to the temperature decrease is schematically depicted in Fig. 12. From Figs. 3, 11 and 12, it is possible to say that the He I to He II phase transition rate, and the generation rate of counterflow or counter-vortex increase with increase in the magnitude of α. The superfluid counterflow or counter-vortex caused by the effect of superfluidity terms in momentum equations (6) and (7) is conspicuous found when the vaporization with the He I to He II phase transition is generated. From Fig. 10, it is found that the gas phase is accelerated in longitudinal and radial directions, not only by the buoyancy force but also due to the negative liquid phase pressure gradient, temperature gradient, and additional lift forces that act on the bubbles. Contrarily, the gas phase is decelerated due to the additional drag forces and positive liquid phase pressure gradient that act on the bubbles.

The several body force effects caused by superfluidity on gas phase velocity $\boldsymbol{v}_g$ are shown in Fig. 13. Case (a)

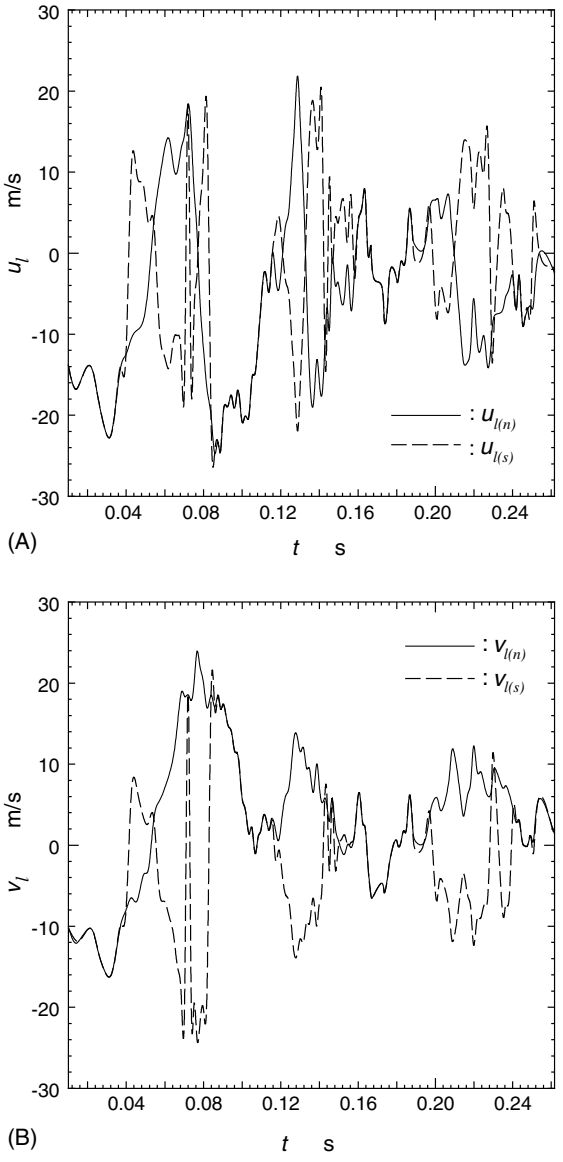

Fig. 11. Normal fluid and superfluid velocity fluctuations as a function of time (A) r-direction component, (B) z-direction component.

means the effect of pressure gradient. Case (b) means the effects of temperature gradient force with case (a). Case (c) means the effects of momentum energy gradient force with case (b). And case (d) means the effects of mutual friction interaction with case (c). These forces are based on the superfluidity terms that appear in momentum Eqs. (6) and (7).

Fig. 14 shows the fluctuation of the normalized liquid phase temperature gradient, $\nabla T_l^* = \nabla T_l / \nabla T_{l(m)}$, as a function of the time, where $\nabla T_{l(m)}$ denotes the time averaged mean value of ∇T_l in prescribed computational time interval. According to Figs. 13 and 14, it is found that the driving force on bubble due to pressure gradient is most dominant compare to other forces, however, the magnitude of fluctuation of $\boldsymbol{v}_g$ correspond to the fluctuation of the temperature gradient ∇T^*. Concerning with Figs. 6–9, it is clarified that the effects of temperature gradient (b), additionally (c), (d), (e) on $\boldsymbol{v}_g$ become larger with increase in the void fraction, or with increase in He I to He II phase transition rate.

The mechanisms of the effects of pressure gradient or temperature gradient that act on the bubbles are schematically summarized in Fig. 15. From Figs. 10, 14 and 15, the temperature gradient force acts opposite direction on normal fluid and superfluid each other, simultaneously, the force oppositely acts on the bubbles in normal fluid and in superfluid mutually. Namely, the bubbles in normal fluid accelerate in the positive temperature gradient direction, and bubbles in the superfluid accelerate in the negative temperature gradient direction. With time, the gas phase motion exhibits diffusing behavior caused by the interaction between the fluid flow of the gas and liquid phases. One of the momentum interactions related to the diffusing behavior is caused by the change of pressure or temperature gradient, which acts on the bubbles due to the superfluid counterflow against the normal fluid. The generation of the normal fluid disturbance also causes the gas phase diffusion. The rate of gas phase velocity deceleration concurrent with He I to He II phase transition, increases with the decrease in the negative liquid phase pressure gradient or the increase of positive pressure gradient, and the positive temperature gradient surrounding the interface between gas and liquid phases. The change of the liquid phase pressure gradient for $\boldsymbol{v}_g$ deceleration with the effect of the spread of the gas phase is caused by the increase of the superfluid counterflow to normal fluid with phase transition.

3. Conclusion

The axisymmetric two-dimensional characteristics of the cavitating flow of liquid helium in a pipe near the λ point were numerically investigated to realize the further development and high performance of superfluid cooling system or new cryogenic engineering applications. First, the governing equations of the cavitating flow of liquid helium based on the Eulerian–Lagrangian unsteady multi-fluid model were presented and several flow characteristics were numerically calculated, taken into account the effect of superfluidity. The main results obtained here can be summarized as follows.

(1) It was found that the characteristics of superfluidity are conspicuous in the large gas phase volume fraction region where the phase change with cavitation

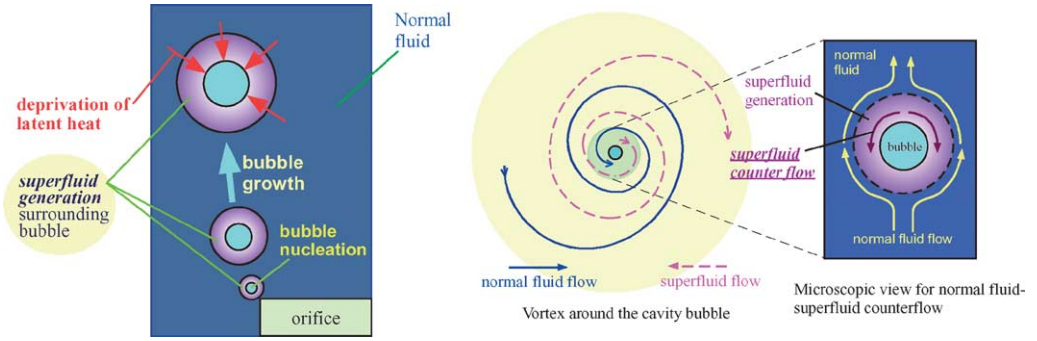

Fig. 12. Schematic of mechanism of the superfluid counterflow or counter-vortex generation.

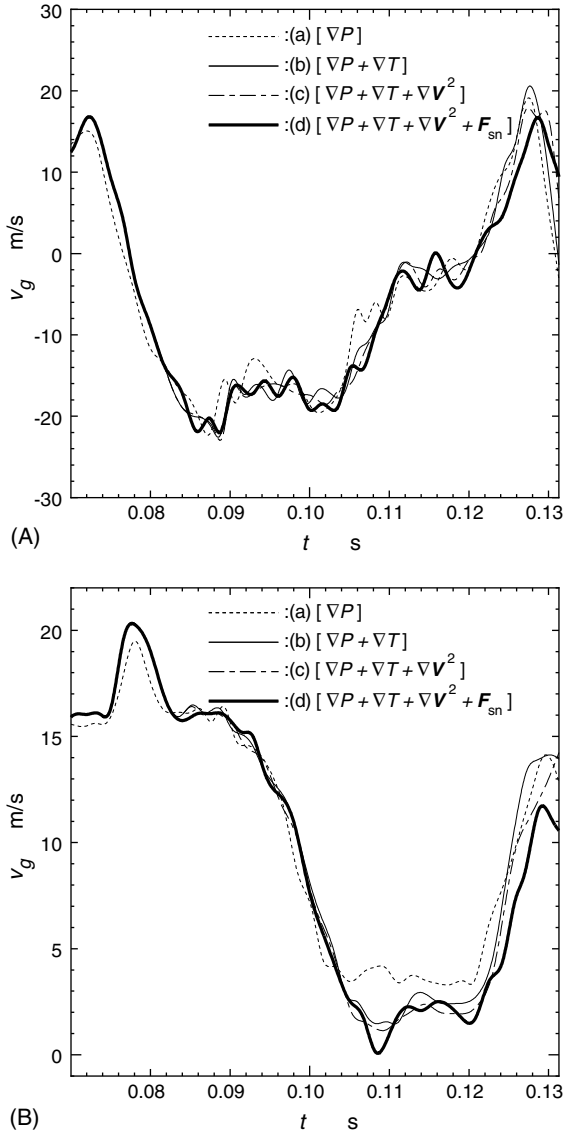

Fig. 13. Several body force effects caused by superfluidity on gas phase velocity (A) r-direction component, (B) z-direction component.

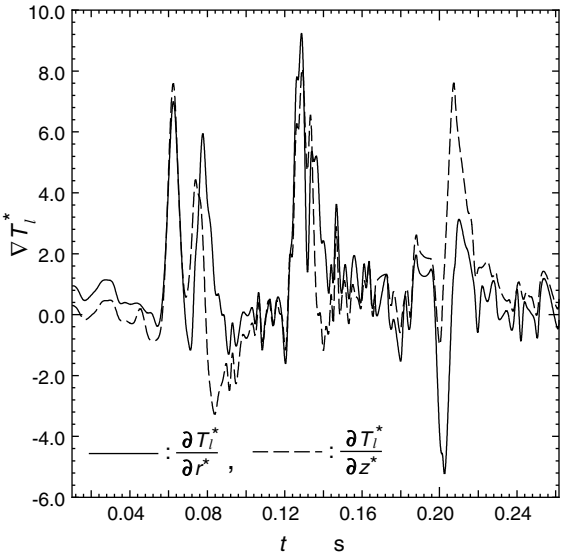

Fig. 14. Fluctuation of the normalized liquid phase temperature gradient as a function of time.

actively occurs and the pressure gradient actively changes. Also, the effect of superfluidity with He I to He II phase transition is mainly caused by the decrease in liquid phase temperature or internal energy due to the deprivation of latent heat for vaporization from the liquid phase.

(2) The superfluid counterflow or counter-vortex against normal fluid caused by the thermomechanical effect of momentum terms based on superfluidity is conspicuous found when the vaporization with He I to He II phase transition is generated. Furthermore, it was found that the gas phase diffusing behavior with time was dominated not only by the change of pressure gradient but also by the change of the temperature gradient that acts on the bubbles due to the superfluid counterflow.

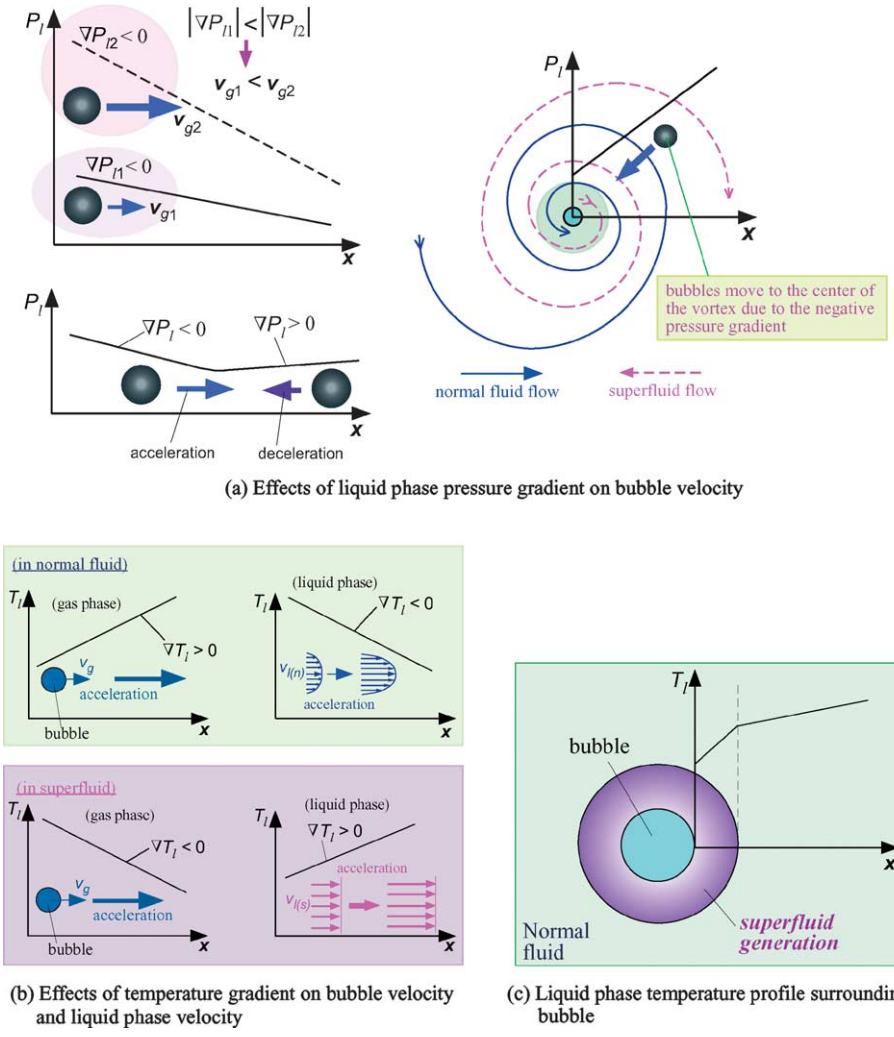

(a) Effects of liquid phase pressure gradient on bubble velocity

(b) Effects of temperature gradient on bubble velocity and liquid phase velocity

(c) Liquid phase temperature profile surrounding bubble

Fig. 15. Mechanism of the effects of pressure gradient or temperature gradient that act on bubbles.

Acknowledgements

The author would like to thank Prof. Masahide Murakami (University of Tsukuba, Japan) for his helpful discussions. This work is supported by an assistance from the grant-in-aid for Scientific Research (C. no. 15760099) by the Ministry of Education, Science and Culture, Japan.

References

[1] N.N. Filina, J.G. Weisend, Cryogenic Two-Phase Flow, Camb. Univ. Press, New York, 1996, pp. 20–76.
[2] R.F. Barron, Cryogenic Heat Transfer, Taylor & Francis, Philadelphia, 1999, pp. 143–213.
[3] S.W. Van Sciver, Helium Cryogenics, Plenum Press, New York, 1996, pp. 77–139.
[4] C.L. Tien, A. Majumdar, F.M. Gerner, Microscale Energy Transport, Taylor & Francis, Washington, DC, 1998, pp. 187–226.
[5] K. Kamijo, M. Yoshida, Y. Tsujimoto, Hydraulic and Mechanical Performance of LE-7 LOX Pump Inducer, J. Propulsion Power 9 (6) (1993) 819–826.
[6] T. Ishii, M. Murakami, Temperature measurement and visualization study of liquid helium cavitation flow through venturi channel, Adv. Cryog. Eng. 47B (2002) 1421–1428.
[7] D.E. Daney, Cavitation in flowing superfluid helium, Cryogenics 28 (1988) 132–136.
[8] S.W. Van Sciver, Heat and mass transfer process in two phase He II/vapor, Cryogenics 39 (1999) 1039–1046.
[9] M. Oike, T. Tokumasu, K. Kamijo, Observation of helium two-phase flow in a pipe, Proceedings of the Fourth

International Symposium on Cavitation, Pasadena, CA, 2001 (in CD-ROM).
[10] J. Ishimoto, M. Oike, K. Kamijo, Two-dimensional numerical analysis of boiling two-phase flow of liquid helium, JSME Int. J. 43B (1) (2000) 62–70.
[11] I. Kataoka, A. Serizawa, Basic equations of turbulence in gas–liquid two-phase flow, Int. J. Multiphase Flow 15 (5) (1989) 843–855.
[12] F.H. Harlow, A.A. Amsden, Numerical calculation of multiphase fluid flow, J. Comput. Phys. 17 (1975) 19–52.
[13] S. Yamamoto, H. Hagari, M. Murayama, Numerical simulation of condensation around the 3-D wing, Trans. Jpn. Soc. Aeronaut. Space Sci. 42 (138) (2000) 182–189.
[14] J.B. Young, Two-dimensional, nonequilibrium, wet-stream calculations for nozzles and turbine cascades, J. Turbomach. 114 (1992) 569–579.
[15] C.F. Barenghi, R.J. Donnelly, W.F. Vinen, Friction on quantized vortices in helium II. A review, J. Low Temp. Phys. 52 (1983) 189–247.
[16] I.L. Bekarevich, I.M. Khalatnikov, Phenomenological derivation of the equations of vortex motion in helium II, Sov. Phys. JETP 13 (3) (1961) 643–646.
[17] A. Kashani, S.W. Van Sciver, J.C. Strikwerda, Numerical solution of forced convection heat transfer in He II, Numer. Heat Transfer Part A 16 (1989) 213–228.
[18] G.K. Batchelor, An Introduction to Fluid Dynamics, Camb. Univ. Press, New York, 1967, pp. 246–255.
[19] A. Tomiyama, I. Zun, H. Higaki, Y. Makino, T. Sakaguchi, A Three-dimensional particle tracking method for bubbly flow simulation, Nucl. Eng. Design 175 (1997) 77–86.
[20] J.O. Hinze, Turbulence, second ed., McGraw-Hill, New York, 1975, pp. 460–471.
[21] Y. Murai, Y. Matsumoto, Numerical study of the three-dimensional structure of a bubble plume, Trans. ASME, J. Fluids Eng. 122 (2000) 754–760.
[22] T.R. Auton, J.C.R. Hunt, M. Prud'homme, The force exerted on a body in invisid unsteady non-uniform rotational flow, J. Fluid Mech. 197 (1988) 241–257.
[23] R. Clift, J.R. Grace, M.E. Weber, Bubbles, Drops, and Particles, Academic Press, San Diego, CA, 1978, pp. 97–141.
[24] H. Lambaré, P. Roche, S. Balibar, H.J. Maris, O.A. Andreeva, C. Guthmann, K.O. Keshishev, E. Rolley, Cavitation in superfluid helium in the low temperature limit, The Eur. Phys. J. B 2 (1998) 381–391.
[25] F. Caupin, S. Balibar, Cavitation pressure in helium, Phys. Rev. B 64 (2001) 064507.
[26] F. Dobran, Liquid and gas-phase distributions in a jet with phase change, Trans. ASME, J. Heat Transfer 110 (1988) 955–960.
[27] C.W. Solbrig, J.H. McFadden, Lyczkowski, E.D. Hughes, Heat transfer and friction correlations required to describe steam–water behavior in nuclear safety studies, AIChE Symp. Ser. 74 (174) (1978) 100–128.
[28] C.W. Hirt, N.C. Romero, Application of a Drift Flux Model to Flashing in Straight Pipes, Los Alamos Scientific Laboratory Report, LA-6005-MS, 1975.
[29] J. Maynard, Determination of the thermodynamics of He II from sound–velocity data, Phys. Rev. B 14 (9) (1976) 3868–3891.
[30] J.S. Brooks, R.J. Donnelly, The calculated thermodynamic properties of superfluid helium-4, J. Phys. Chem. Ref. Data 6 (1) (1977) 51–104.
[31] R.D. McCarty, Thermodynamic Properties of Helium II from 0 K to the Lambda Transitions, NBS Technical Note, TN-1029, 1980.
[32] C.A. Moses, G.D. Stein, On the growth of steam droplets formed in laval nozzle using both static pressure and light scattering measurements, Trans. ASME, J. Fluids Eng. 100 (1978) 311–322.
[33] A. Tomiyama, M. Hirano, An improvement of the computational efficiency of the SOLA method, JSME Int. J. 37B (4) (1994) 821–826.
[34] A.A. Amsden, F.H. Harlow, The SMAC method: A numerical technique for calculating incompressible fluid flows, Los Alamos Scientific Laboratory Report, LA-4370, 1970.